ELSEVIER

Classification of Multispectral Images Based on Fractions of Endmembers: Application to Land-Cover Change in the Brazilian Amazon

John B. Adams,[*] Donald E. Sabol,[*] Valerie Kapos,[†] Raimundo Almeida Filho,[‡] Dar A. Roberts,[,††] Milton O. Smith,[*] and Alan R. Gillespie[*]*

Four time-sequential Landsat Thematic Mapper (TM) images of an area of Amazon forest, pasture, and second growth near Manaus, Brazil were classified according to dominant ground cover, using a new technique based on fractions of spectral endmembers. A simple four-endmember model consisting of reflectance spectra of green vegetation, nonphotosynthetic vegetation, soil, and shade was applied to all four images. Fractions of endmembers were used to define seven categories, each of which consisted of one or more classes of ground cover, where class names were based on field observations. Endmember fractions varied over time for many pixels, reflecting processes operating on the ground such as felling of forest, or regrowth of vegetation in previously cleared areas. Changes in classes over time were used to establish superclasses which grouped pixels having common histories. Sources of classification error were evaluated, including system noise, endmember variability, and low spectral contrast. Field work during each of the four years showed consistently high accuracy in per-image classification. Classification accuracy in any one year was improved by considering the multiyear context. Although the method was tested in the Amazon basin, the results suggest that endmember classification may be generally useful for comparing multispectral images in space and time.

[*] Department of Geological Sciences, University of Washington, Seattle

[†] Department of Plant Sciences, University of Cambridge, United Kingdom

[‡] Instituto Nacional de Pesquisas Espaciais, São Jose Dos Campos, SP, Brazil

[††] Present address: Department of Geography, University of California at Santa Barbara.

Address correspondence to John B. Adams, Dept. of Geological Sciences, Univ. of Washington, Seattle, WA 98195.

Received 10 March 1994; revised 1 November 1994.

INTRODUCTION

For certain remote-sensing applications, such as monitoring environmental change, it is essential to be able to compare classes from image to image. In spite of successes in classifying some individual multispectral images using conventional supervised or unsupervised techniques, it has been difficult to obtain consistent classes from images taken at different times, owing to variability in illumination, atmospheric effects, and instrumental response. As a result, with a few exceptions (e.g., Hall et al., 1991; Lucas et al., 1993), monitoring of changes in land cover by remote sensing typically has been restricted to measurements of changes in spatial patterns, and less attention has been given to spectral changes.

Long-term monitoring of changes in vegetation cover in the Amazon Basin has been focused primarily on the removal of forest cover, rather than on more subtle changes in land use or vegetation cover. Brazil's space agency, Instituto Nacional de Pesquisas Espaciais (INPE), has acquired Landsat data through its own receiving station since 1975, and, despite frequent cloud cover in the Amazon region, these images comprise a rich historical record of deforestation and land use in Amazonia. INPE monitors deforestation by analyzing Landsat Thematic Mapper (TM) color composites of Bands 3, 4, and 5 (e.g., INPE, 1992). Skole and Tucker (1993) compiled a large-area mosaic of Landsat TM Band 5 images to assess deforestation and habitat fragmentation in the Brazilian Amazon between 1978 and 1988.

There has been little work on regrowth or land-use changes within the cleared areas in Amazonia, although such information is vital to assessments of biomass and

REMOTE SENS. ENVIRON. 52:137–154 (1995)

655 Avenue of the Americas, New York, NY 10010

0034-4257 / 95 / $9.50
SSDI 0034-4257(94)00098-8

carbon cycling. Lucas et al. (1993) addressed this problem in a study of the same area north of Manaus that was studied in this article. They applied a minimum-distance classifier to four time-series TM images using Bands 3, 4, and 5 to define three broad categories of land cover for each date: primary forest, secondary forest, and agricultural land. Changes in land cover in the TM images and in two older MSS images were used to estimate the ages of secondary forests. The study by Lucas et al. (1993) illustrates both the importance of using time-series Landsat (or other multispectral) data, and the limitations inherent in applying traditional statistically based spectral classifiers to such images.

In our study we tested a fundamentally different way of classifying multispectral (and hyperspectral) images based on spectral mixture analysis (SMA) (e.g., Adams et al., 1986, 1993; Smith et al., 1990a,b; Gillespie et al., 1990). Encoded-radiances (DNs) in all bands were transformed to fractions of reference endmembers, which are reflectance spectra of well-characterized materials that mix to produce spectra equivalent to those of pixels of interest in an image. Endmember fractions are easier to interpret than DNs, and, therefore, provide a more intuitive link between image measurements and observations in the field. For example, field observers readily understand the significance of a pixel having 65% green vegetation and 35% soil, but have more difficulty interpreting the equivalent band-radiance values. Classes were defined as domains of fractions of endmembers; thus, classes were defined in a physical context, such as the amount of green vegetation, rather than on statistically defined clusters of data points.

The SMA-based classification was tested on a time series of Landsat TM images in the context of an ongoing multidisciplinary study of hydrology and land-use change in the Brazilian Amazon. The joint Brazilian–U.S. project is part of NASA's Earth Observing System (EOS) program. One aspect of the study is to measure long-term environmental changes, including natural processes (Batista et al., 1993; Nelson et al., 1994; Nelson, 1994), and anthropogenic activities of deforestation, agriculture and urbanization (e.g., INPE, 1992; Skole and Tucker, 1993; Shimabukuro et al., 1994; Fearnside, 1993 and references cited therein).

Adams et al. (1990) compared calibrated TM images for August 1988 and August 1989 of the area north of Manaus, and demonstrated that the primary forest and different communities of regrowth vegetation could be described by variations in the fractions of spectral endmembers: green vegetation (GV), nonphotosynthetic vegetation (NPV; e.g., bark), and shade. Additional categories of land use were discriminated when soil was included in the analysis. Adams et al. (1990) also showed that temporal changes on the land surface (as documented by field observations) were accompanied by variations in the fractions of the endmembers. The present study extended this analysis to two additional images of the same area (August 1990 and August 1991) and developed the SMA-based classification of the four-image time series. The results of spectral classification of this time series are presented to illustrate the methodology and to show details of land-use change. The ecological and hydrological implications of land-use change in this area will be published separately, as will a more complete record of deforestation and land use since the mid 1970s.

METHODS

Field Observations and Measurements

The area north of Manaus (Fig. 1) is still dominated by primary forest, but clearing for cultivation and pasture has occurred locally since the late 1970s, especially along the main road (BR 174) leading north to Boa Vista. Field observations were made by one or more of the authors within 1–4 weeks of the time of acquisition of each of the TM images (August 1988, 1989, 1990, and 1991). They were concentrated at two cattle ranches, Fazenda Dimona and Fazenda Esteio, which are ca. 70 km north of Manaus along the BR 174 (Fig. 1), and include research areas of the Biological Dynamics of Forest Fragments Project (BDFFP) of the National Institute for Research in Amazonia (INPA) and the Smithsonian Institution (Lovejoy and Bierregaard, 1990; Bierregaard et al., 1992). Because of their uneven management histories (Bierregaard et al., 1992), these ranches include a wide range of vegetation from well maintained pasture through regrowth to primary forest (Lucas et al., 1993). The rectilinear layout of the ranches and the small, regular forest fragments of the BDFFP-facilitated location and orientation on the images and in the field.

Each year both sites were photographed on the ground and from light aircraft, and additional air observations and photographs were made of much of the area extending northwards between Manaus and the Balbina reservoir. Reflectance spectra from 400 nm to 1000 nm were obtained for materials in the field using Spectron Engineering and Analytical Spectral Devices hand-held spectroradiometers. Spectral and photographic measurements of primary forest canopy were made at two 40-m research towers operated by INPA, one at Reserva Ducke and one at Bacia Modelo. Samples of soils and dry vegetation were collected and measured in the laboratory at the University of Washington over the wavelength range 400–2500 nm using a modified Beckman total-hemispherical spectroreflectometer.

Image Calibration

Time-of-flight system and atmospheric calibration data were not available for Landsat images of the study area, nor was it possible to calibrate empirically to ground targets at the time of each overpass of the satellite. A

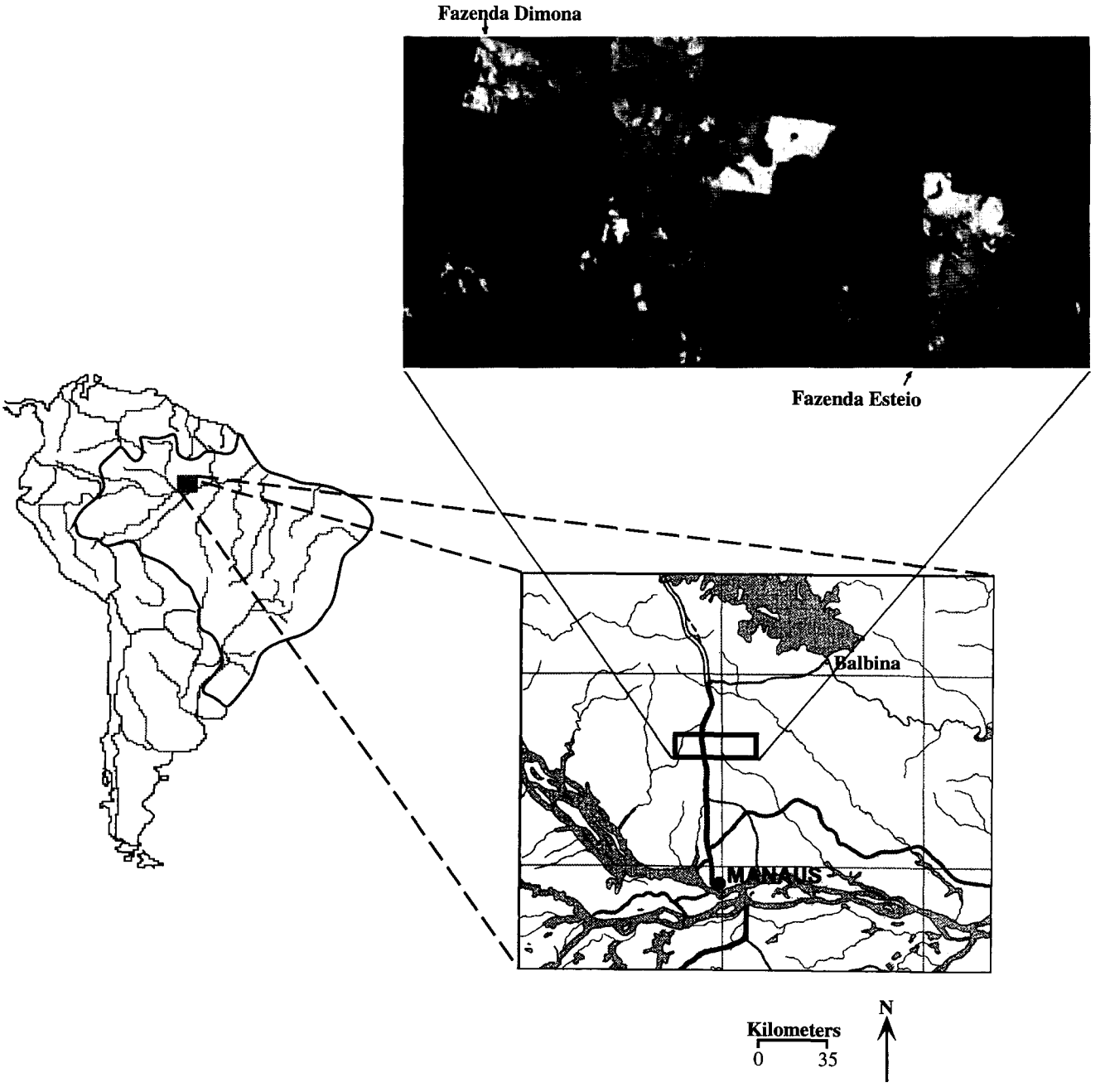

Figure 1. Index map of study area. Landsat Thematic Mapper (TM) subscene of ranches (fazendas) that include the Biological Dynamics of Forest Fragments Project. The subscene is 1234 pixels by 604 pixels, with a horizontal dimension of approximately 40 km. Fazenda Dimona, the cleared, rectilinear area on the west side of the image, is shown enlarged in Figures 7 and 9.

nominal calibration to reflectance using preflight instrument calibration data and a standard atmospheric model was not made, because the accuracy of these corrections could not have been verified and any errors in calibration might have propagated undetected into the classification (Sabol et al., 1992a,b; Smith et al., 1994a,b).

The 1989 image was calibrated using a modified empirical-line method (Roberts et al., 1993) and by the spectral mixture analysis method (Smith et al., 1990a; Gillespie et al., 1990; Adams, 1993). The other three images were inter calibrated to the 1989 image using training areas known to be temporally invariant. The intercalibration of these images was similar to the approach used by Hall et al. (1991) where they applied a "radiometric rectification" to allow a comparison of classes from two Landsat images taken at different times. How-

Table 1. Combined Gains and Offsets to Convert Encoded Radiance (DN) to Reflectance in Each of the Four TM Images[a]

	15 Aug 1988		*02 Aug 1989*		*21 Aug 1990*		*08 Aug 1991*	
Band	*Gain*	*Offset*	*Gain*	*Offset*	*Gain*	*Offset*	*Gain*	*Offset*
TM1	224.39	47.770	226.71	44.110	226.71	44.110	150.85	65.150
TM2	191.68	10.130	191.39	9.250	191.39	9.250	114.16	23.130
TM3	271.59	3.805	271.74	3.240	271.74	3.240	157.98	20.150
TM4	218.49	10.300	205.90	12.280	205.90	12.280	124.53	34.470
TM5	292.57	9.260	267.74	9.030	267.74	9.030	249.38	13.230
TM7	138.18	0.086	137.74	0.086	137.74	0.086	133.58	0.767

[a] The 1989 image was calibrated to reflectance by empirical-line and mixture-model methods (see text); the other three images were intercalibrated to the 1989 image. For each band: reflectance = (DN – offset) / gain.

ever, the Hall et al. (1991) supervised classification did not require an absolute calibration to reflectance. In the present study it was essential to calibrate to reflectance to permit the images to be analyzed within the framework of reference endmembers consisting of laboratory and field reflectance spectra.

Table 1 gives the gain and offset that was applied to each band of the four images to convert DN to reflectance. Each gain and each offset combines multiple effects, including those contributed by the instrument and atmosphere. Calibrations were applied uniformly to each image, and did not take into account variability in the atmosphere across individual images.

A major source of spectral variability from one image to another in a time series is illumination differences associated with variations in solar elevation and azimuth and local incidence angle. Although variations in illumination within each image that are caused by macrotopography can be removed if a satisfactory photometric function is combined with digital terrain-elevation models, suitable topographic data were not available for the area studied. The effects of illumination differences were minimized by comparing images of the same area that were all acquired in August of successive years. Furthermore, the topographic relief in the study area is low, although there is shadowing along ravines, and associated with vegetation canopies.

Illumination variations caused by topography and roughness at all scales (including subpixel "texture") were incorporated into the endmember "shade" in a spectral mixture analysis, discussed below. Shade was used as one basis for classification, as will be discussed; however, shade also was removed from the images by rescaling the fractions of the endmembers after deleting the shade.

Endmembers, Fractions, and Residuals

Mixed pixels and the concept of endmember proportions were recognized in early studies of multispectral images (e.g., Horowitz et al., 1971). Subsequently, several approaches to unmixing multispectral images have been explored, and there is a rapidly growing literature. [See, for example, references cited in Adams et al. (1993).] Most studies of unmixing have used uncalibrated spectra derived from training areas on images (image endmembers). When relatively pure, image endmembers may model mixed pixels within one image; however, uncalibrated, image-derived endmembers also may change from image to image in a time series. To monitor spectral changes over time, it is essential to delineate invariant laboratory or field reflectance spectra (reference endmembers).

Spectral mixture analysis differs from many other applications of linear mixing to multispectral images in that it links image spectra to laboratory reflectance spectra of materials that comprise most reference data sets. Thus, as used in this article, SMA is an analytical framework within which images are calibrated to reflectance, and pixels are modeled as potential mixtures of selected laboratory or field spectra. All endmember spectra may mix with shade, to simulate spectral variations in illumination caused by topography and surface texture. This evolving technique has been applied in various contexts (e.g., Adams et al., 1986, 1989, 1993; Smith et al., 1990a,b; 1994a,b; Gillespie et al., 1990; Roberts et al., 1993).

In our study image endmembers were selected as a first step; then reference endmembers were found, along with combined gains and offsets for each band to calibrate the image to reflectance. Image endmembers were chosen either from training areas on the image or by stepwise analysis of each pixel. All six reflective bands were used. Image endmembers consisted of spectra (in DN) which, when mixed, produced spectra that fit many other pixels in the image. Image endmembers represented spectral extremes in the image, but only those that participated in mixing. Thus, for example, the spectrum of a body of water is distinct and "pure" (not a mixture), but it was not a useful endmember for the rest of the image, because pixels containing water occurred only locally. DNs for each pixel were converted to fractions of image endmembers using Eq. (1) and solving the

pseudoinverse matrix (Golub and Van Loan, 1989). Fractions of endmembers summed to 1 for each pixel.

$$DN_i = \sum_{k=1}^{n} f_{ik} DN_{ik} + \varepsilon_i \quad \text{and} \quad \sum_{k=1}^{n} f_k = 1, \qquad (1)$$

DN_i = encoded radiance in band i for each pixel,
DN_{ik} = encoded radiance in band i for each image endmember k,
f_{ik} = fraction of each image endmember k calculated band by band,
i = band number,
k = each of n image endmembers,
ε_i = remainder between measured and modeled DN ("band residual").

Image endmembers themselves were redefined as mixtures of reference endmembers, which were derived from a set of laboratory or field spectra measured in units of reflectance. Reference endmembers were selected from spectra of materials occurring in the study area, and from other relevant spectra. For example, spectra of forested areas typically could be fit by mixtures of laboratory or field spectra (reference spectra) of green vegetation, nonphotosynthetic vegetation, and shade. Image endmembers were described in terms of reference endmembers by

$$DN_{ik} = g_i' \sum_{j=1}^{n} f_{ijk} R_{ij} + o_i' + \varepsilon_i \quad \text{and} \quad \sum_{j=1}^{n} f_j = 1, \qquad (2)$$

DN_{ik} = encoded radiance in band i for each image endmember k,
f_{ijk} = fraction of each reference endmember j that contributes to k, calculated band by band,
R_{ij} = reflectance in band i for each reference endmember j,
ε_i = remainder between measured and modeled DN,
g_i' = gain for band i,
o_i' = offset for band i.

Image endmembers were calibrated to reflectance using Eq. (2) by calculating the combined gains and offsets for each band. The values found for the gains and offsets are given in Table 1, and can be used to calibrate all pixels to reflectance, assuming a spatially uniform atmosphere. In the rest of this article, the term "endmember" means "reference endmember."

In addition to fractions of the endmembers, band residuals were calculated for each pixel. The band residual is the difference between the measured and the modeled DN in each band. Residuals over all bands were summarized as a root-mean-squared (RMS) "error." The overall fit of the model was judged to be "good" if: 1) Band residuals and/or RMS error were low, and 2) fractions were not < 0 or > 1. Pixels having high RMS values and/or fractions < 0 or > 1 indicated unmodeled compositional variability in the scene. The simple endmember model applied here was not expected to fit all pixels. The physical significance of fraction and RMS departures from the simple model was evaluated within a spatial context by displaying fractions, RMS-error values, and (in a few cases) band residuals as images. Such images could have been used to guide further analysis by applying multiple sets of endmembers (Sabol et al., 1992b; Roberts et al., 1992; Adams et al., 1993), or foreground/background analysis (Smith et al. 1994a,b). However, the added compositional information that would have been gained from these techniques was not needed to produce the basic classification discussed in this article.

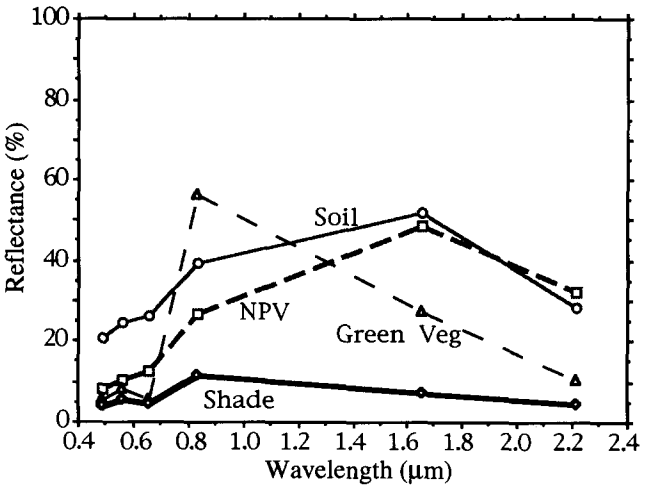

Figure 2. TM pseudospectra of reference endmembers. Pseudospectra of green vegetation, nonphotosynthetic vegetation, and soil were derived from laboratory reflectance spectra by application of the full TM filter functions. Shade spectrum was derived from shadowed pixels in the calibrated 1989 TM image.

Systematic errors occurred in estimates of the fraction of green vegetation when the linear mixing model was applied. Nonlinear mixing effects, largely introduced by transmission of light through green leaves at near infrared wavelengths, are well documented (e.g., Roberts et al., 1990; 1993), but were judged to be small enough to ignore for the purposes of the simple model applied here.

RESULTS

Number and Variability of Endmembers

The same four (reference) endmembers, shade, green vegetation (GV), nonphotosynthetic vegetation (NPV), and soil (Fig. 2) were used to model all of the images used in this study. It was recognized that four spectra were inadequate to describe the full range of natural variability of materials on the ground. The selected endmembers were proxies for three broad kinds of spectrally distinct materials (plus shade). It is not appropriate to interpret them in a more specific context, for

example, as a vegetation species. Shade included light scattered and / or transmitted by green vegetation (Roberts et al., 1993), and was not simply a photometric shade having zero reflectance in all bands.

Endmembers were selected from a computer library of spectra by applying Eq. (2). It is possible that other spectra not included in our collection might provide an equally good or better fit to the images. Variations in the endmember spectra affected estimates of fractions; however, classification results were relatively insensitive to small variations in the endmembers. An important function of the selected endmembers was to provide a consistent frame of reference for analysis of the four images.

The fraction images and the RMS-residual images show that the closed-canopy vegetated areas that dominate the study area were well modeled by the basic endmembers GV, NPV, and shade (Fig. 3). In these areas where no soil was exposed, the band-residual images revealed spectral variability in the vegetation itself; however, this variability was near the level of system noise, as expressed by banding and speckle. Field observations confirmed that the main differences among vegetation communities were the variable fractions of the endmembers. For example, the primary forest was characterized by relatively high fractions of shade and NPV.

Shade was an important parameter for distinguishing different vegetation types. The primary forest had the highest shade fraction because canopy roughness produces self shadowing. Second-growth vegetation dominated by *Cecropia* and *Vismia* was characterized by smoother canopies, and had a lower shade fraction. Areas that were clear of vegetation, or that were covered by Kudzu vine, had the lowest amount of shade. The topographic effects of shade are visually apparent (Fig. 3).

When relative fractions of the endmembers for each TM date were compared with field and aircraft observations, pixel-to-pixel variability in the endmembers was consistent with qualitative and semiquantitative field data. Quantitative measurements of the fractions proved to be impractical. For example, the felling of trees and shrubs produced a ground cover dominated by woody material in trunks and branches, and dead or dying leaves. The exposure of these materials (here termed "slash"), along with litter and some soil, was accompanied by an obvious decrease in the fractions of GV and shade, and an increase in NPV and soil. Although the absolute fractions, in principle, could have been measured by line transects or quadrats, in fact it was not feasible to make such measurements for several pixel-sized areas (30 m × 30 m) over a tangled mass of downed trees and branches. Primary forest presented a similar problem, in that the fraction of NPV includes trunks, branches, and stems over a wide range of spatial scales in a rough and largely inaccessible canopy. NPV and green vegetation were estimated from observations and photographs of forest canopy from a 40-m tower, and from many low-altitude color aerial photographs; however, quantitative measurements at all scales, especially over an area of several pixels, were impractical within the scope of the field program.

Temporal Variations in Endmember Fractions

The 1988, 1989, 1990, and 1991 TM images were coregistered, and the fractions of each endmember were compared among years. Qualitative changes in the fractions were displayed as color composites, using three images at a time (Fig. 4 and Table 2). In three-year color composite images, major changes in fractions have the most saturated colors, whereas minor changes produced less saturated colors, and gray tones indicate no temporal change.

Interpretation (Table 2) was based on an experiential assessment of changes in the individual endmembers. For example, in the NPV image (Fig. 4), red signifies a large increase in the fraction of NPV in 1990 relative to the previous two years. Field experience indicated that cutting of vegetation was the most common way that NPV was increased by a large amount inside and bordering the previously cleared areas. This interpretation was tested by examining the other endmembers. Support for the interpretation of cut vegetation was found when the same pixels that showed a large increase in NPV in 1990 also showed a large decrease in GV and in shade, and a small increase in soil. Each of these relative changes was consistent with cutting of vegetation. Other interpretations were derived similarly from the basic data shown in Fig. 4 and Table 2. Fine details of clearing and regrowth of vegetation are shown in the color composites. Locally, many of these changes were confirmed by field and aircraft observations.

Color composites revealed subtle relative changes in the proportions of the endmembers; however, it was difficult to quickly render a visual interpretation of all of the colors on these images without using a key. Furthermore, color composites are limited to three images. To show changes over more than three images, it is necessary to establish a classification.

Classification

The first step in the classification procedure was to define areas on the images that corresponded to known types of land cover, based on field observations. Mean values of the fractions of the four endmembers were measured for representative areas on the images. Mean values for several types of land cover are plotted in Figure 5a. They are representative of, but do not define the limits of, the prospective classes. Class names were selected to have significance to an observer in the field

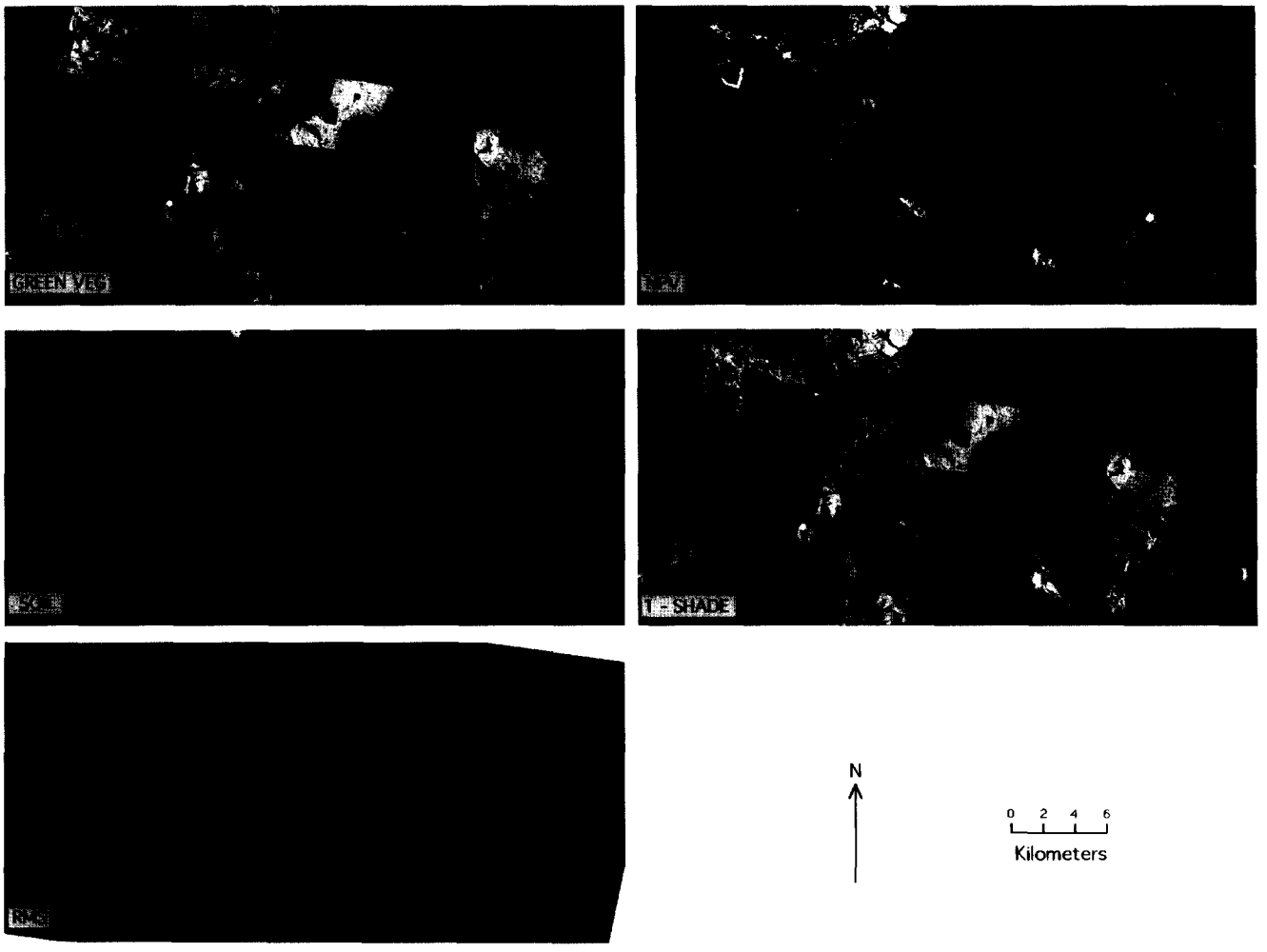

Figure 3. Fraction images and the RMS-residual image for the 1990 TM subscene. Green veg (GV) = green vegetation; NPV = nonphotosynthetic vegetation; RMS = root mean squared "error". Fractions are scaled to pixel lightness. Lighter pixels indicate more of the endmember, except that the scheme is reversed for 1-Shade, so that pixels with a higher shade fraction are darker, to convey a more intuitive image of topographic shading. The RMS image is strongly contrast stretched, and illustrates that the mean residuals for the well-modeled parts of each image are near the level of the system noise, which is expressed by banding and speckle.

in the context of this study (Adams et al., 1989; 1990; 1993).

The second step in the classification was to define the limits of each class. Fractions of the four endmembers for each pixel were displayed as a data cluster on a modified tetrahedron (Fig. 5b) that could be rotated on the computer screen to show any desired projection. Class boundaries in the data space were established by an interactive process of color-highlighting on projections of the data cluster, on histograms of the individual endmembers, and on the images. Data points highlighted on any one representation of the data were simultaneously displayed on the others (Buja et al., 1987; 1991). Although only the 1990 subscene was used in Figure 5, all TM images were used to establish class boundaries, because the best example of classes sometimes occurred in different images. This empirical method assured that all well understood areas on the image were correctly located in the data cluster.

A satisfactory segmentation of the data cluster and the image required that boundaries be established sequentially, and in a particular order. First, the data were divided into two categories based on the shade fraction. In the August images studied, a fraction of 0.53 (hereafter referred to as 53%) shade separated primary forest from other types of land cover, the primary forest having the higher shade fraction. A subsequent step subdivided the $<53\%$-shade pixels having no soil into levels of NPV relative to GV. The remaining $<53\%$-shade pixels were then categorized based on GV, NPV, and soil

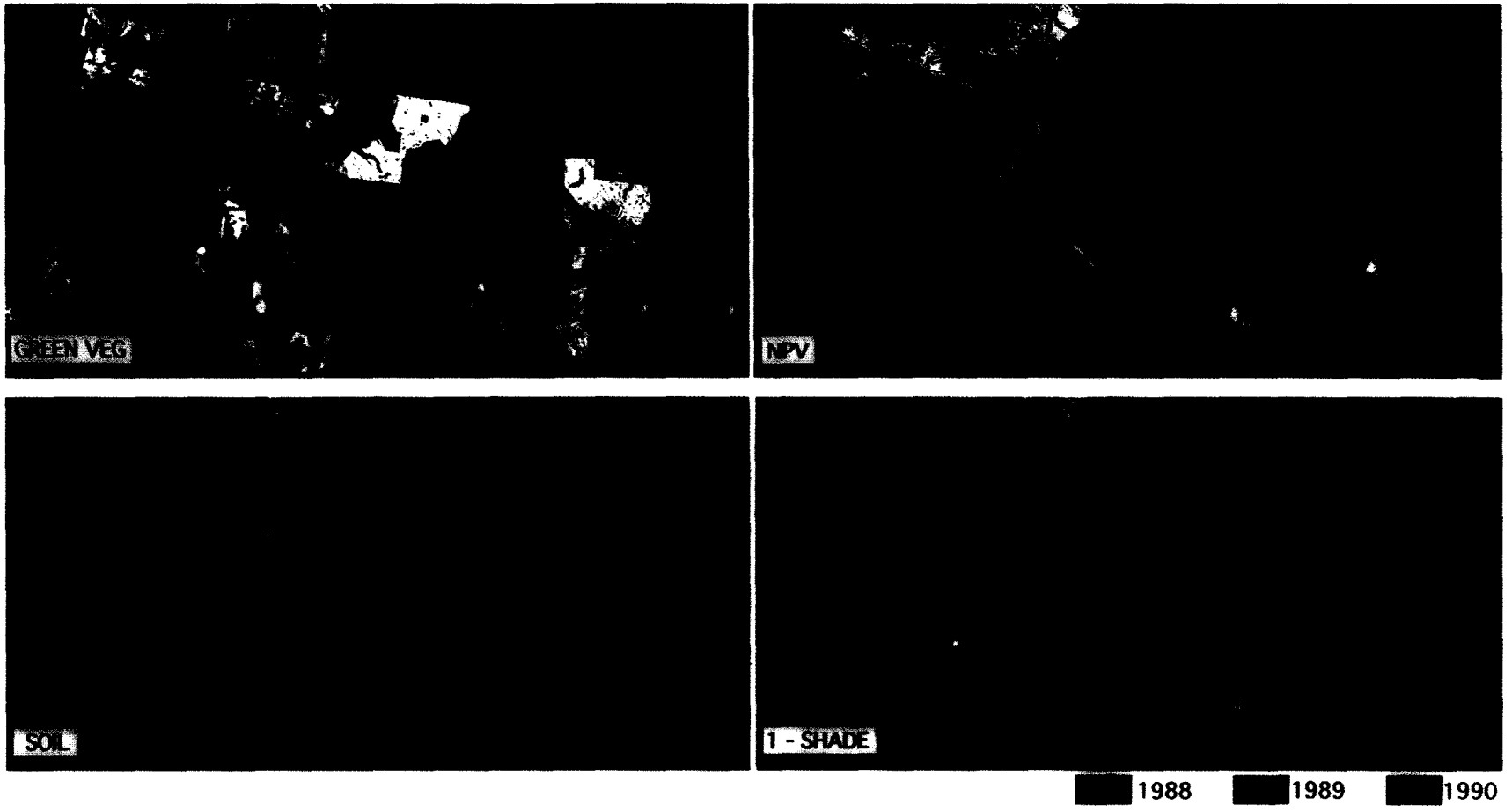

Figure 4. Three-year color composite images of endmember fractions. Blue = 1988, green = 1989, red = 1990. See Table 2 for interpretation of colors.

Table 2. Interpretive Color-Key for Multitemporal Fraction Images[a]

NPV Soil	*Green Veg Shade*	*Interpretation*
White / gray	White / gray	No change from 88 to 89 to 90
Red (R)	Cyan (− R = G + B)	Cleared in 90
Green (G)	Magenta (− G = R + B)	Cleared in 89; regrowth in 90
Blue (B)	Yellow (− B = R + G)	Clear in 88; regrowth in 89 and 90
Cyan (− R = G + B)	Red (R)	Clear in 88; still clear in 89; regrowth in 90
Magenta (− G = R + B)	Green (G)	Clear in 88; regrowth in 89; cleared again in 90
Yellow (− B = R + G)	Blue (B)	Cleared in 89; still clear in 90

[a] Red = 1990; green = 1989; blue = 1988. More saturated colors = greater change from year to year. White / gray tones = no change from year to year. Lighter tones = more of endmember. Darker tones = less of endmember.

Figure 5. a) Mean values of fractions of several types of land cover, measured on areas in the images that were well characterized by ground observations. The ternary diagram defines the proportions of GV, NPV, and soil. The length of the vertical bar and its number defines the fraction of shade. b) Scattergrams of fractions of the four endmembers for the 1990 subscene. Fractions are displayed on projections of modified tetrahedra. The population of pixels is strongly concentrated where the clusters are darkest. A small population of pixels extends outside the triangles (fractions < 0 or > 1). These "overflow" pixels do not fit the sample model based on the four endmembers, indicating different compositions, misregistrations at sharp boundaries, or noisy pixels. Overflow pixels on the scattergrams were displayed on the images for evaluation of their spatial context.

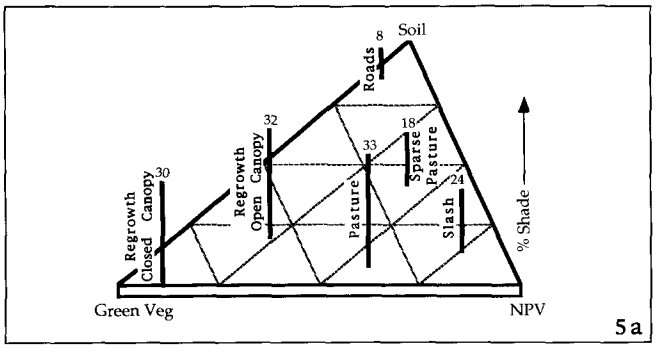

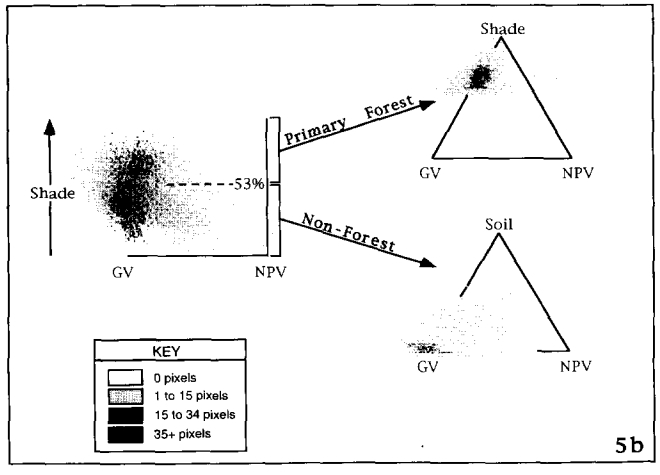

fractions. Subclasses of forest are not discussed in this article.

Because the shade fraction varies with sun elevation and azimuth, shade cannot be included as a field attribute when classifying land cover. Nonforest pixels were categorized after removing shade by resumming to 1 the fractions of GV, NPV, and soil (Figs. 5 and 6). Normalization "removes" shade by apportioning the shade fraction to the other endmembers. Although normalization removes shading well, it is only an approximation in the case of shadows (Adams et al., 1993). Classes that were defined by normalized fractions were minimally influenced by illumination and topography, making it possible, in principle, to define the same classes in any image, regardless of illumination conditions.

By defining classes in terms of fractions of endmembers it was possible to predict where most types of land cover would occur in the data space (Figs. 5 and 6). Predictions were checked using known training areas, and were consistently correct as long as the field area could be described in terms of the abundances of the four endmembers. Thus it was possible to classify types of land cover for which there were no known training areas. For example, during early analysis of the 1988 image there was no field-verified example of a forested area that had just been cut, and had not been burned that would provide a training area for the class "Slash." It was evident, however, that Slash should have a very low fraction of GV, a high fraction of NPV (bark, wood, and dry leaves), and a low fraction of soil. Thus, an estimate was made as to where the class Slash would occur on Figures 5 and 6. This prediction was proved correct when a good example of Slash appeared on the 1990 image, and its identity was verified in the field.

Nomenclature and Spectral Mimicking

The nomenclature for the classes (Table 3) represents a level of abstraction beyond that of the endmembers. Because each class name was selected to have significance to an observer in the field, each carries strong spatial implications that dominate the spectral ones. For example, few observers have a mental image of a TM spectrum of a forest, whereas most know what a forest

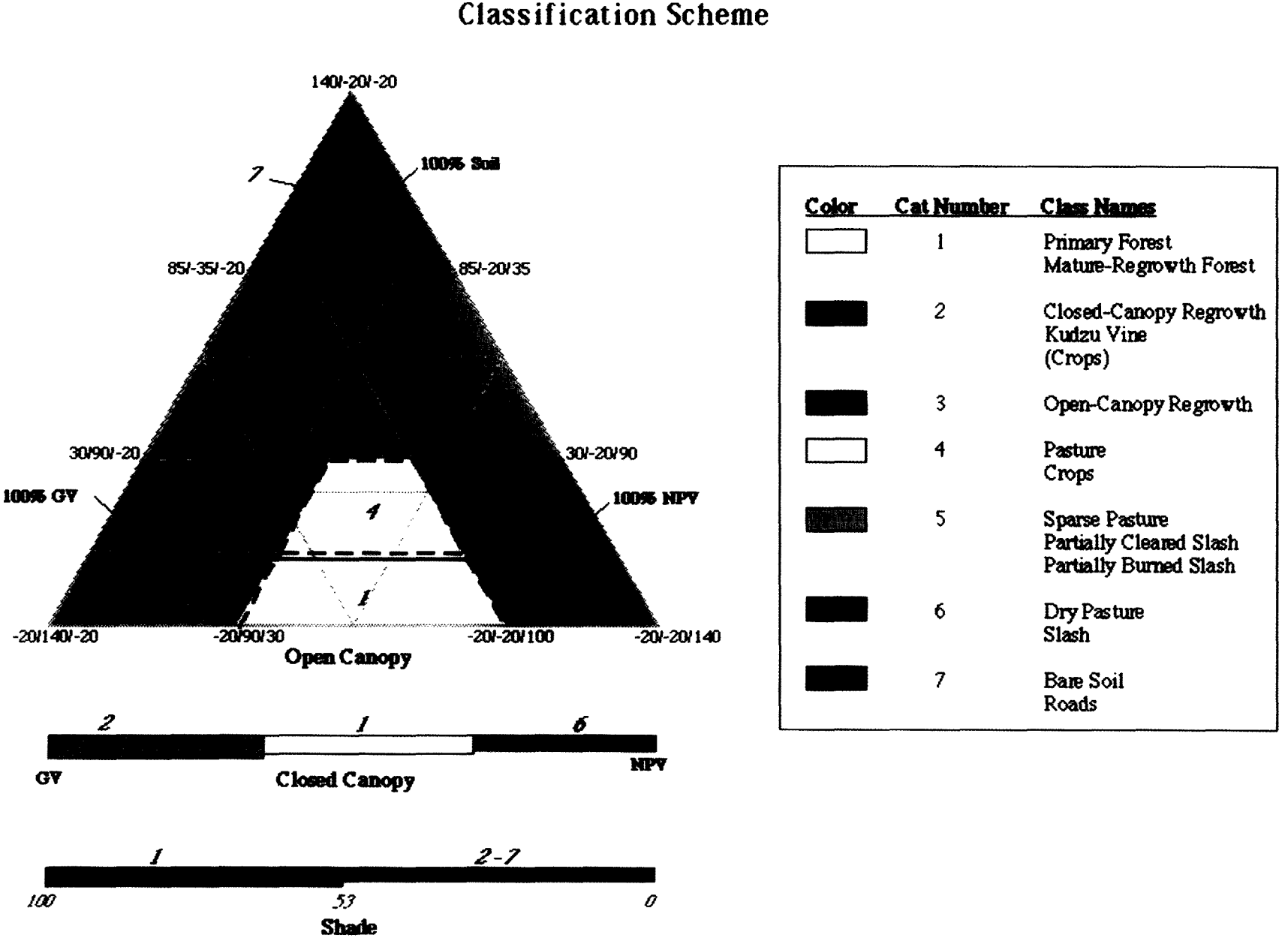

Figure 6. Classification diagram. Lower bar segregates pixels according to shade fraction alone. Colored bar divides low-shade fraction into GV and NPV fractions; only pixels with 0–0.02 soil are categorized (± 2% soil is within measurement error). The ternary diagram divides the remaining pixels, based on GV, NPV, and soil fractions. Inner, solid triangle encloses fractions between 0 and 1. Outer triangle encloses fractions < 0 and > 1. Numbers refer to category boundaries. Key at right shows class names associated with fraction categories.

Table 3. Fraction Categories and Class Names

Fraction Category Number	*Class Names*	*Description / Comments*
1	Primary Forest	High shade, 30–80% NPV as stems, branches, bark; minor exposure of leaf litter, bark in gaps; no detectable soil
	Mature Regrowth Forest	
	Burned fields, partly vegetated	High shade mimicked by black charcoal; 30–80% NPV as dead wood; no detectable soil
2	Closed-Canopy Regrowth	Shrubs and / or trees; low shade; <30% NPV as stems, branches, bark; no detectable soil
	Kudzu Vine (or Crops)	Very low shade; <30% NPV; vine used as ground cover to suppress shrub regrowth, no crops in study area
3	Open-Canopy Regrowth	Shrubs and / or trees; low shade; <30% NPV in canopy as stems, branches, bark, and as ground-litter; soil detectable but <30% exposed
4	Pasture	Moderate shade; high shade for tall, upright grass; 30–80% NPV as dry grass, and wood as trunks and stumps; <30% soil
	Crops	Very low to moderate shade; 30–80% NPV as leaf / stalk litter; <30% soil; minor in study area
5	Sparse Pasture	Low shade; >30% exposed soil; 0–70% NPV as dry grass, dead wood
	Partially Cleared Slash	Low shade; >30% soil, 0–70% NPV as dry leaves, branches, bark, wood (slash) partly obscured by green vegetation
	Partially Burned Slash	Low to high shade; charcoal may mimic high shade; soil and NPV same as for Partially Cleared Slash
	Crops	Low shade; >30% soil; 0–70% NPV as leaf / stalk litter; none in study area
6	Dry Pasture	Low shade; >50% NPV as dry grass, dead wood; <30% soil
	Slash	Low shade; >50% NPV as dead leaves, stems, branches, bark, and wood
7	Bare Soil	Low shade; >80% soil; agricultural or construction areas
	Roads	Low shade; >80% soil; unpaved

looks like in the field. To judge whether a pixel was correctly classified spectrally required that the spectral and spatial information be reconciled.

There is no *a priori* reason why class names that are based on field (spatial) observations should have unique fractions of endmembers, anymore than they should have unique combinations of DN values. Endmember fractions, therefore, cannot always be inverted to unique class names. Nevertheless, in the Amazon context, the endmember fractions for each pixel corresponded to a small number of possible classes, as is shown in Table 3. Additional information was needed to decide among the possible choices of classes, as is discussed below.

To avoid premature selection of specific class names, all classes that mimicked one another were grouped and labeled by numbered category (Fig. 6). For example, based on the four endmembers, which included only one type of NPV, it was not possible to distinguish between the classes Slash and Dry Pasture; therefore a numbered category was established that included both. In this example the ambiguity could be resolved in several ways: 1) by introducing additional endmembers for NPV that distinguished between dry grass and bark / wood / dry leaves (see Methods section); 2) by historical context; for example, if the pixel were known to have been Primary Forest shortly before changing to Slash or Dry Pasture, it would more likely be Slash; 3) by outside information and / or field context.

Temporal Changes in Classes

Changes on the ground from one year to another were accompanied by predictable changes in the representative fractions of the endmembers, as was shown in the color composite images (Fig. 4). Changes occurred either as a "jump" from one set of representative fractions to another, such as from Primary Forest to Slash, or as a partial shift of the fractions resulting in a small translation within the data tetrahedron (Figs. 5 and 6). Classification changes were recorded whenever fraction values crossed class boundaries.

Class changes for Fazenda Dimona are shown in Figure 7. From visual comparison alone it is evident that, over the 3-year period from August 1988 to August 1991, there were significant changes in the amount of cleared land relative to the area covered by second-growth vegetation. The data were used to make quantitative assessments of changes in individual classes, and in groups of classes (Fig. 8). Interpretation of the changes in land cover is deferred to a separate article.

Pixel Histories and Superclasses

Using the coregistered, classified images for the four years, temporal changes were recorded for each pixel, to establish historical records. Changes in class assignments implied that specific processes had affected the land cover. For example, a change from Pasture to Open-Canopy Regrowth implied growth of shrubs, and an attendant lack of maintenance of the pasture. Most pixels could be classified at a higher level on the basis of their history, as was done by Adams et al. (1990) using just the 1988 and 1989 images. Thus, a pixel that had the class history (in these images) of Primary Forest → Slash → Pasture, could be assigned a new class name such as "forest converted to pasture." Another

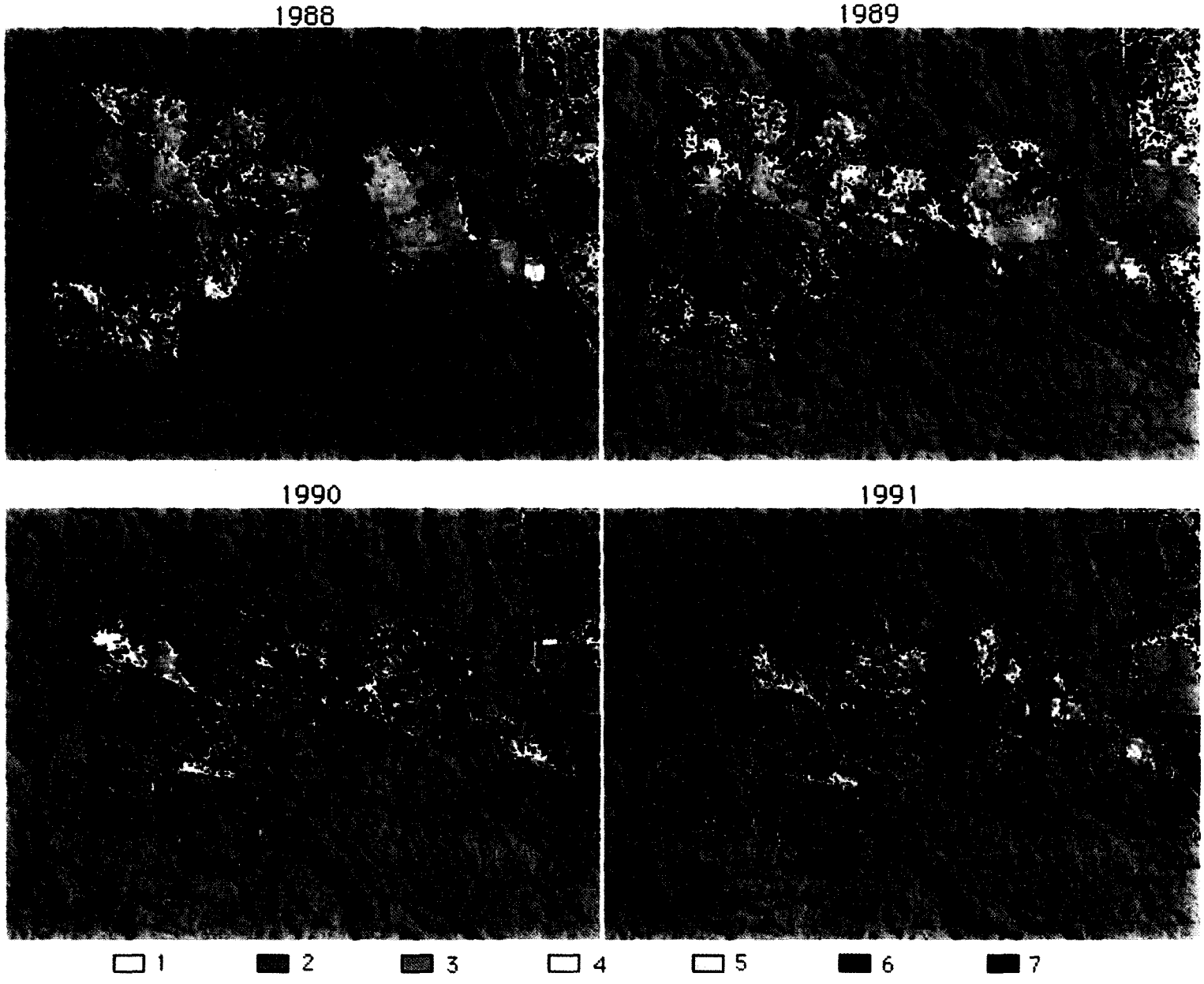

Figure 7. Endmember-fraction classification of 1988, 1989, 1990, and 1991 TM subscenes of Fazenda Dimona. Area shown is in the upper left corner of Figures 3 and 4. Colors (see Fig. 6) designate fraction categories. Many of the yellow (Cat. 4) and brown (Cat. 5) pixels of pasture in 1988 and 1989 are replaced by blue (Cat. 3) and green (Cat. 2) regrowth pixels in 1990 and 1991. Corridor cut in primary forest in 1990 (bottom of subscene) consists of Cats. 5 and 6. From context and ground observations the applicable classes are Partially Cleared or Burned Slash and Slash. Black areas are ponds (all images) or recent burns (1991 only).

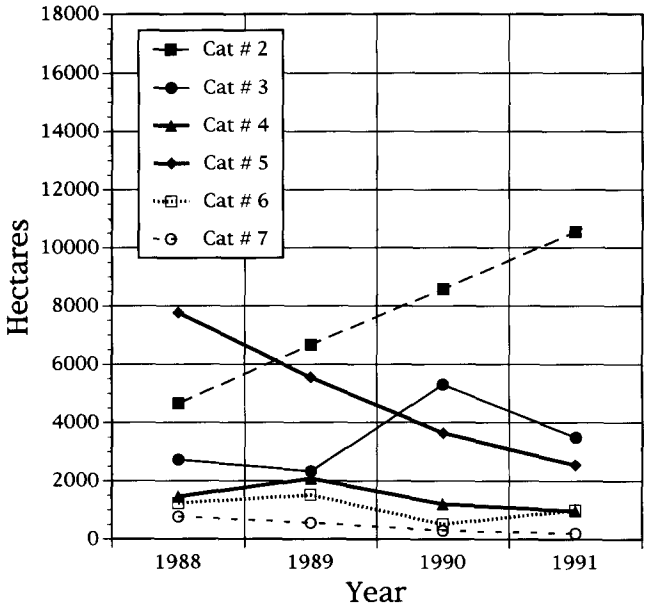

Figure 8. Quantitative changes in classes for Fazenda Dimona (same subscene as Fig. 7) from 1988 to 1991. Fraction Categories are defined in Table 3 and in Figure 6. Pasture decreased from 7700 ha to 2500 ha; closed-canopy regrowth increased from 4500 ha to 10,500 ha.

pixel might have the history: Pasture → Open-Canopy Regrowth → Closed-Canopy Regrowth, and could carry a new class name such as "overgrown pasture." Higher-level classes were termed "superclasses." Formal names were not given to superclasses, because there are many possible pixel histories over the elapsed 3-year period, and the utility of any superclass depends on the local context and on the objectives of the study. Superclasses were displayed by assigning distinctive colors to pixels having similar class histories, and superposing the color information on a reference image, such as a shade-complement image (Fig. 9).

Class changes (Fig. 10) could occur between two, three, and four images (one, two, and three time-intervals, respectively). Because class changes have specific implications regarding processes on the ground they must be interpreted in context with field and other evidence, and the time associated with each process must be considered. For example, 3 years are not enough to measure a change from pasture to primary forest; however, many other changes were found to occur over a period of 1 year, including transitions from cleared areas to closed-canopy regrowth. Thus, even the images spaced at 1-year intervals do not necessarily record all of the class changes that are associated with surface processes. Unrecorded classes may be implied from the recorded class changes. If the recorded class change is from forest to closed-canopy shrubs, there may even have been multiple cycles of clearing and regrowth that occurred between images. Although this history is not recorded, there is a minimum implied history (Fig. 10) of intermediate stages of Slash, Partially Cleared Slash, and Open-Canopy Shrubs.

As mentioned earlier, some of the ambiguities in class names (Table 3) were resolved by using the pixel histories. Some histories, and thus some superclasses, are not possible within the context of the area or the time covered by the images. For example, the fractions of the basic endmembers did not distinguish between Sparse Pasture and Partially Cleared Slash. These classes commonly could be resolved, however, by referring to the previous class in a time series. A sparse pasture can be produced by overgrazing, which increases the amount of soil exposed, but slash cannot be produced from pasture without first passing through a stage of shrub growth.

Class histories were used to address specific questions about land use in the study area. For example, the class-change data were used to show: 1) felling of forest and clearing of regrowth that occurred between 1988 and 1991 (Fig. 9a) and 2) where pasture had been overgrown by shrubs and trees during the same interval (Fig. 9b). From Figure 9 it is evident that at Fazenda Dimona, during the time interval studied, more area of pasture was lost to regrowth than was cleared.

Areas of felled forest (red in Fig. 9a) were determined by grouping all pixels that were in the class Primary Forest in 1988, 1989, or 1990, and changed to Slash, Partially Cleared Slash, Partially Burned Slash, Pasture, Sparse Pasture, or Open-Canopy Regrowth. Similarly, pixels of felled regrowth (blue in Fig. 9a) were defined as having been Open-Canopy Regrowth or Closed-Canopy Regrowth in 1988, 1989, or 1990 and changed to Slash, Partially Cleared Slash, Partially Burned Slash, Pasture, or Sparse Pasture. Areas of regrowth of shrubs (green in Fig. 9b) were determined by grouping pixels that were Pasture or Slash in 1988, 1989, or 1990 and changed to Open-Canopy Regrowth or Closed-Canopy Regrowth.

DISCUSSION

Sources of Error in Classification by Fractions of Endmembers

As described above, pixels that were classified by endmember fractions could fit more than one class as defined by (nonspectral) attributes in the field. Mimicking was addressed by first placing the endmember fractions in a numbered category, and, in a subsequent step, selecting a class name from the numbered category, based on context or other information. This approach did not result in misclassification, as long as the potential for mimicking was recognized (e.g., Slash or Sparse Pasture). Misclassification could occur, however, at the stage of interpretation where, for example, context is used to select the class name "Slash."

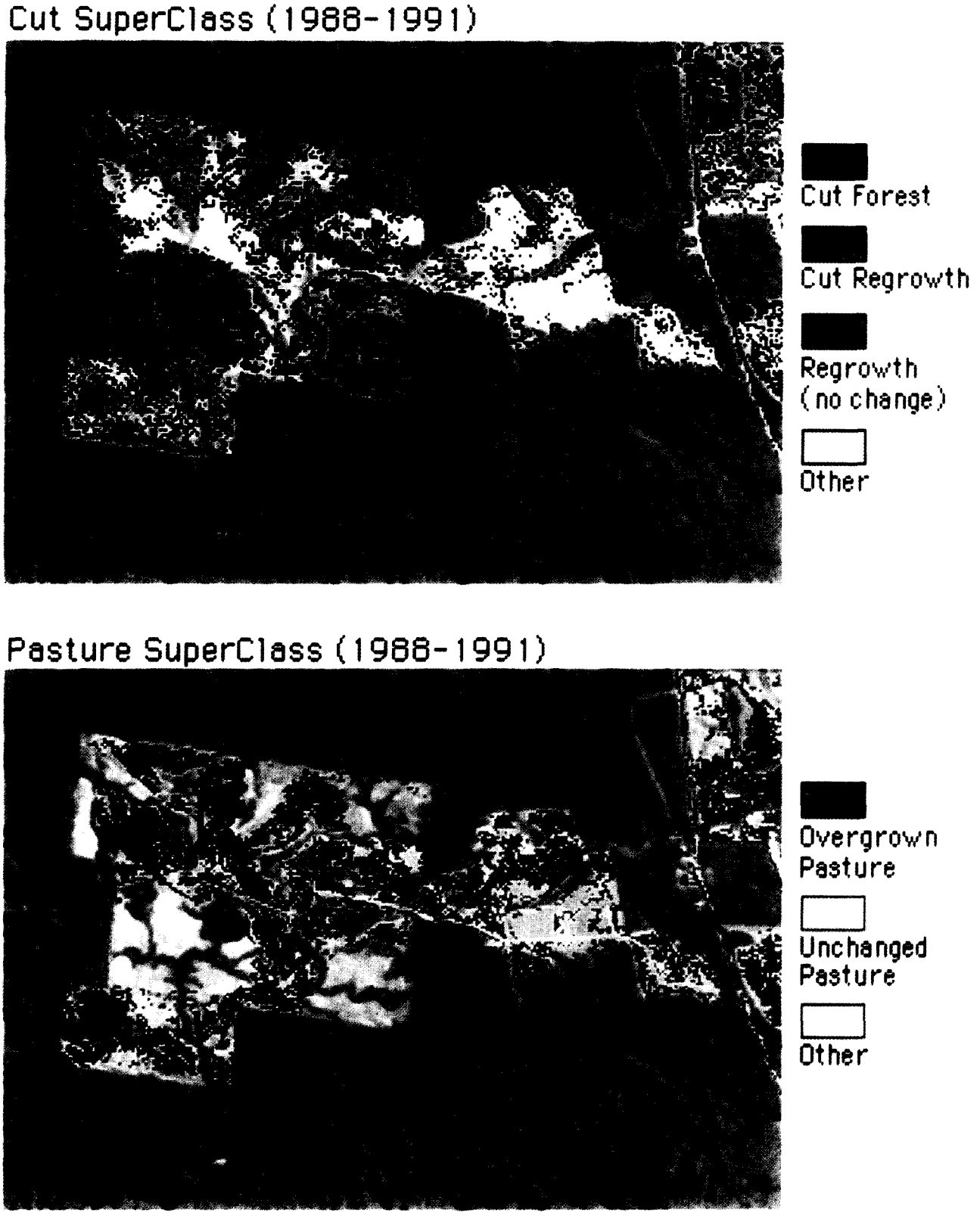

Figure 9. Superclasses. a) Cut superclass. Image shows a cumulative record of clearing at Fazenda Dimona for 1988 to 1991. Green = regrowth unchanged; blue = regrowth → any class except Forest; red = Forest → any other class; gray = all other pixels. Image illustrates that relatively little regrowth was cleared to maintain pastures. b) Pasture superclass. Image shows a cumulative record of regrowth. Yellow = unchanged pasture; green = Pasture → Open-Canopy Shrubs or Closed-Canopy Regrowth; gray = all other pixels. Image indicates that more pasture was overgrown than maintained. Colors are superposed on 1-Shade image (darker = more shade).

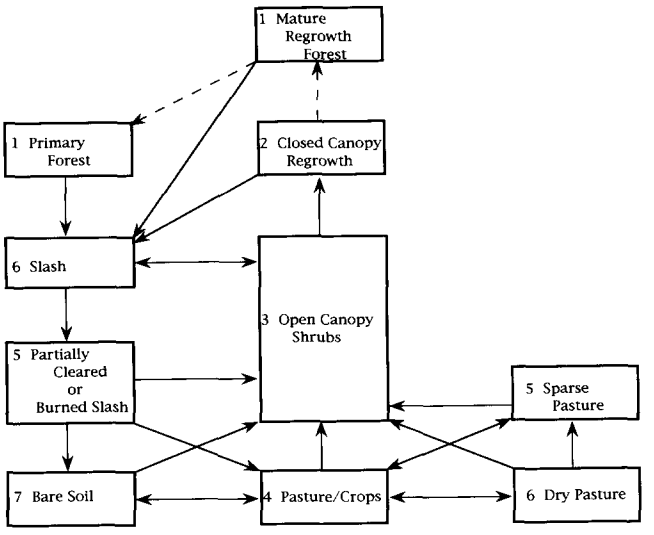

Figure 10. Pathways for class changes, based on knowledge of processes in the study area. Numbers in boxes refer to categories (Table 3 and Fig. 6). Images are not expected to record all steps. Arrows indicate direction(s) of change. Dashed arrows indicate slow processes that would not be revealed in the 3-year image sequence. Disallowed changes (1–3 years) include: primary forest → mature regrowth forest; all classes → primary forest or mature regrowth forest.

Misclassification also could occur when endmembers were mimicked by other spectra. This type of error could be avoided by knowing in advance what endmembers were spectrally similar. For example, it was apparent at the stage of selecting reference endmembers (see Methods section) that some soils mimicked some dry grasses. In the case of TM this potential ambiguity cannot be resolved except by context; however, Roberts et al. (1992; 1993) and Sabol et al. (1992b) showed that dry grass and soil could be distinguished in California with high spectral resolution Airborne Visible-Infrared Imaging Spectrometer (AVIRIS) images.

In one case misclassification occurred when a cluster of pixels fit the endmember model, but their field class was not included on the class list, along with their spectral attributes. Field checks revealed that these pixels covered areas where Kudzu vine, that had been planted as a cover crop, mimicked the fractions characteristic of closed-canopy *Cecropia* forest. Subsequent analysis showed that these areas had a lower shade fraction than *Cecropia*, and could be correctly classified on that basis.

Mimicking also occurred when field classes, like endmembers, were mixed at the subpixel scale. The classes selected for this study were appropriate for the 30-m pixels of TM, for at this spatial scale large groups of pixels corresponded to the field-defined class names, and relatively few pixels were large enough to occupy more than one class. Where pixels overlapped class boundaries in the field, there was no corresponding class name, and the pixels typically were misclassified. As a result, misclassification was more likely to occur at sharp spatial boundaries such as roads and edges of fields. Misclassification at boundaries is a general problem that affects any classification scheme. It is not due to an error in the fractions of the endmembers. If one were to visit the pixel on the ground the proportions of shade, GV, NPV, and soil would be expected to be accurate within the limitations of the model used.

It follows from the above discussion that any increase in pixel size may increase classification error. The effect of increasing pixel size was simulated by adding blocks of pixels, and classifying the resulting images. As expected, classification accuracy relative to the starting image decreased rapidly. At the scale of hundreds of meters, many pixels overlapped the spatial boundaries of the classes that were defined in the field; therefore, the pixels were misclassified. The evident exception was the class Primary Forest, which comprised large enough areas to be classified correctly in most pixels.

System Noise Propagating to Fraction and Class Errors

Fraction errors are a complex function of system noise, spectral contrast, spectral sampling, and residuals, and they may propagate into a classification. The magnitude of these errors was assessed using methods developed by Sabol et al. (1992a,b), Smith et al. (1994b), and Lawler and Adams (1994). Based on the uncertainty in the fractions derived from multiple applications of Eq. (1), the corresponding error in the classes was calculated, and a confidence level was assigned to each pixel (Sabol et al., 1992a,b). Pixels falling below the 90% confidence level in terms of their numbered category assignment were displayed as an image (not shown) and on the modified tetrahedron of the data cluster (Figs. 5 and 6). The spatial pattern of the pixels below the 90% confidence limit was used to judge whether there were significant areas of the image that were not well classified, or whether poorly classified pixels were associated with systematic or random noise.

Low confidence levels were associated with pixels near category boundaries in the data space (Fig. 6), where relatively small influences on the signal by system noise could cause pixels to move to an adjacent, but incorrect, category. For a given level of system noise this effect was calculated independent of the particular image, and provided a basis for predicting which classes could be recognized most reliably in the context of the others (Sabol et al., 1992). For example, the lowest spectral contrast among the four endmembers was between NPV and soil. Therefore, the below-90%-confidence zone was wider for those category boundaries

that are based on distinguishing NPV from soil, whereas they were narrower for the boundaries between GV and NPV, or GV and soil. Accuracy near category boundaries was improved by using pixel histories (time-series images) to identify misclassified pixels. Pixels that showed disallowed transitions according to Figure 10 were reassigned to the nearest neighboring class.

At any given level of system noise, the ability to distinguish among GV, NPV, and soil was influenced by the shade fraction. Increased shade fractions were accompanied by reduced signal levels from other endmembers, eventually to the point where noise exceeded a preselected confidence-level threshold for the signal, and classification was no longer possible. The threshold signal (and shade fraction) could be calculated for each pixel by the method of Sabol et al. (1992a) mentioned above. A simple, qualitative display of the effects of shade on classification confidence is shown in Figures 7 and 9, in which the classification images are modulated by the complemented shade image. Pixels having low shade fractions were distinctly colored, whereas high-shade pixels were dark, and the colors associated with the class assignments were faint or indistinct to the eye. Thus, pixels that were misclassified because of low signal-to-noise also were too dark to identify by color.

Classification Accuracy

Classification accuracy traditionally is expressed as the percentage of correctly classified pixels. Assessment of accuracy requires sampling a statistically significant number of pixels, and correctly locating those pixels in the field. However, a single figure for classification accuracy can be misleading if, for example, a large, homogeneous area such as Primary Forest is correctly classified, thereby strongly weighting the total. In this study, no attempt was made to produce a formal measure of the percentage of accurate pixels; however, it is estimated that the figure would be above 90%.

The high estimated accuracy is a consequence of 1) designating a small number of classes that are based on spectrally specific fraction categories; 2) allowing pixels to carry the names of more than one class until context or history information allowed further decision; 3) not forcing pixels with high residuals or high noise to be classified; and 4) flagging and rectifying classification errors by spatial context and by defining forbidden class changes within time-series images.

Shade, Variable Illumination, and Topography

The subdued topography of the study area minimized differences in illumination due to variable local incidence angles. Variation in sun elevation and azimuth also was minimized, because all images were obtained within the same month (August). These conditions were optimum for comparing classifications in a time series. However, these same conditions were not optimum for testing the more general case of endmember classification of a time series, where illumination conditions vary substantially due to topography, and from image to image. Nonetheless, some useful insights emerged that apply to the general case.

The main effect of varying either the topography or image-wide illumination conditions is to change the shade fraction. In this article, shade was evaluated in an image context for each of the TM scenes, and the 53%-shade boundary that separated forest from nonforest was valid for all four of the August images. The shade boundary would be different for other zenith angles, and perhaps for other azimuth directions. Dividing the image into $>53\%$ shade and $<53\%$ shade categories facilitated the subsequent steps, consistent with a typical dichotomous-tree approach. However, it is important to note that $>53\%$ shade did not identify a pixel as primary forest, although most pixels of primary forest had $>53\%$ shade.

A few pixels of nonforest (for example, pasture or regrowth) had $>53\%$ shade, and, therefore, mimicked forest, because they included steep topography, mainly in ravines. (Fortuitously, in the study area primary forest typically was not felled on steep slopes; therefore, few pixels were incorrectly segregated in the first step of the classification procedure). Significantly, pixels of nonforest that were segregated into the high-shade category because of topography usually could be identified correctly by the other fractions. This was done by selecting subcategories of shade (e.g., 53–63%), evaluating the normalized fractions of the nonshade endmembers as previously described (Fig. 6), and displaying those pixels in the image context. Results suggested that the confounding effects of variable illumination on classification could be minimized by successively evaluating the (normalized) nonshade fractions in "slices" of the shade fraction (i.e., in subcategories of shade values), all in an image context.

In all four of the TM scenes a few scattered pixels in the forest were classified as Closed-Canopy Regrowth, because they had low shade ($<53\%$), coupled with high GV and low NPV. Analysis of the time-series confirmed that the same pixels underwent at least one change from Closed-Canopy Regrowth to Primary Forest (a forbidden transition on Fig. 10), thereby indicating a classification error. Closer examination revealed that these pixels occurred on elevated, sun-facing areas of canopy where shadowing was minimal. Once identified they were reclassified as Primary Forest, based on context.

An important refinement of the analysis of the shade fraction would be to discriminate shade produced by macrotopography from shade produced by subpixel topography and roughness associated with canopies. The contribution from subpixel shading and shadowing can be isolated as a remainder after subtracting the shade

fraction derived from a digital-elevation model (macrotopography) from the shade fraction derived from the mixture analysis (Adams et al., 1993). This analysis was not possible for the Amazon study because adequate digital elevation data were not available.

General Significance of Temporal Classification

In this study the endmembers GV, NPV, soil, and shade formed the basis for numbered categories, classes, and superclasses. The endmember spectra selected to model the images comprised a simplistic model of the actual spectral variability, as mentioned in the Methods section. Although this simple model ignored some of the details of spectral variability on the ground, it had the advantage of representing common types of materials that comprised ground cover in part of Amazonia. Furthermore, the endmembers comprised a fixed frame of reference for evaluating changes from image to image.

Because the endmembers used in this study represent basic components of many natural vegetated surfaces, the classification scheme presented here may be broadly applicable in Amazonia and elsewhere, if particular caution is given to how class names are applied. Many types of mature forests worldwide are characterized by high shade and moderate NPV, simply as a consequence of the increasing roughness of canopies and the development of woody tissue as trees mature. When forests are felled, there typically follows a predictable adjustment of the fractions of the basic spectral components: Shade and GV decrease, while NPV and soil increase. Similarly, regrowth in cleared areas typically is expressed by an increase in GV at the expense of NPV and soil.

These are examples of changes in fractions of endmembers that are associated with processes, but that are relatively insensitive (for the case of a simple endmember model) to the species or communities of vegetation involved. Thus, when the same endmembers and categories used in the Amazon study were applied to TM images of forested areas in the state of Washington, USA, the images were surprisingly well modeled. However, the class names, which were based on local context, could not be exported. For example, in the Manaus region studied, most of the clearing of primary forest has been to establish pasture for cattle, or, locally, other agriculture. Some large areas were cut and allowed to revert to second growth without being used. Commercial logging has been absent or negligible in this area. In contrast, in the northwest Washington TM image studied, the forest clearing was related to commercial logging. Thus, endmember fractions in Category 6 (Fig. 6, Table 3) might be interpreted as the class Pasture in the Manaus image, but as a class "Clearcut" in Washington. Furthermore, temporal changes in the Washington forests would lead to superclasses that could have different names from those relevant to Manaus, reflecting the local context. Caution is strongly advised, therefore, when applying class names outside of an area where the context of fraction changes is well understood. These results are beyond the scope of this article, but suggest further work to test the generality of the approach.

SUMMARY AND CONCLUSIONS

The analytical approach presented in this article was developed primarily to monitor change in areas where the spectrally dominant materials on the ground are well understood or can be inferred. It was found that a modest initial investment in measuring the spectra of materials on the ground and / or knowledge of the materials and processes in the area formed a basis for subsequent remote-sensing measurements over time.

A fixed frame of reference for measuring change was established by a simple four-endmember model consisting of green vegetation, nonphotosynthetic vegetation, soil, and shade. Changes in fractional abundances within an image and from image to image reflected biophysical processes and human influences on land use.

Land-cover types and quantitative changes in land cover were measured by classifying images based on endmember fractions. Classification was not based on conventional statistically based techniques or on training areas from each image, although training areas were used initially to establish fraction categories and to link them to class (field) names. Within the limitations of system noise, general categories of land cover were determined with high accuracy. Categories typically included more than one class; therefore, assignment of class names was based on context or pixel history. The spectral history of each pixel, considered together with the spatial context, provided a powerful way to monitor change that extended far beyond what was feasible by ground measurements. The approach described in this article potentially has broad applicability for monitoring detailed changes in land cover.

We thank the Instituto Nacional de Pesquisas Espaciais for providing access to TM images, and the Instituto Nacional de Pesquisas na Amazonia and the BDFF project for facilitating field work. G. Ganade, J. Camargo, B. Nelson, and B. Forsberg helped in the field and with aircraft observations. S. Willis assisted with programming. J. Mustard and an anonymous reviewer provided helpful comments for improvement of the manuscript. Portions of the work were supported by the Biological Dynamics of Forest Fragments Project, the International Atomic Energy Agency, and NASA. A grant from the W. M. Keck Foundation supported development of the analytical technique and funded computer systems.

REFERENCES

Adams, J. B. (1993), A combined atmospheric and systems calibration from spectral mixture analysis, in *Proc. Workshop on Atmospheric Correction of Landsat Imagery* (P. N.

Slater and L. D. Mendenhall, Eds.), Geodynamics Corp., Torrance, CA, pp. 177–180.

Adams, J. B., Smith, M. O., and Johnson, P. E. (1986), Spectral mixture modeling: a new analysis of rock and soil types at the Viking Lander 1 site, *J. Geophys. Res.* 91(B8):8098–8112.

Adams, J. B., Smith, M. O., and Gillespie, A. R. (1989), Simple models for complex natural surfaces: a strategy for the hyperspectral era of remote sensing, *Proc. IGARSS 1989*, Vancouver, BC, Vol. 1, pp. 16–21.

Adams, J. B., Kapos, V., Smith, M. O., Almeida Filho, R., Gillespie, A. R., and Roberts, D. A. (1990), A new Landsat view of land use in Amazonia, *Int. Arch. Photogramm. Remote Sens.* 28:177–185.

Adams, J. B., Smith, M. O., and Gillespie, A. R. (1993), Imaging spectroscopy: interpretation based on spectral mixture analysis, in *Remote Geochemical Analysis: Elemental and Mineralogical Composition* (C. M. Pieters and P. Englert, Eds.), Cambridge Univ. Press, New York, Vol. 7, pp. 145–166.

Batista, G. T., Shimabukuro, Y. E., Lawrence, W. T., and Antunes, M. A. H. (1993), El Niño effect on Amazon vegetation cover through NOAA-AVHRR, in *VI Sociedad de Especialistas LatinoAmericanos en Percepcion Remota (SELPER) Symp.*, Cartagena, October.

Bierregaard, R. O., Jr., Lovejoy, T. E., Kapos, V., dos Santos, A. A., and Hutchings, R. W. (1992), The biological dynamics of tropical rain forest fragments, *Bioscience* 42:859–866.

Buja, A., Hurley, C., and McDonald, J. A. (1987), A "Data Viewer" for multivariate data, in *Computer Science and Statistics: Proc. 18th Symp. on the Interface*, ASA, Washington, DC, pp. 171–174.

Buja, A., McDonald, J. A., and Michalak, J. (1991), Interactive data visualization using focusing and linking, in *Proc. Second IEEE Conf. on Visualization*, San Diego (G. M. Nielson and L. Rosenblum, Eds.), IEEE Computer Soc. Press, New York.

Fearnside, P. M. (1993), Deforestation in Brazilian Amazonia: the effect of population and land tenure, *Ambio* 22:537–545.

Gillespie, A. R., Smith, M. O., Adams, J. B., Willis, S. C., Fischer, A. F., III, and Sabol, D. E. (1990), Interpretation of residual images: spectral mixture analysis of AVIRIS images, Owens Valley, California, in *Proc. 2nd Airborne Visible / Infrared Imaging Spectrometer (AVIRIS) Workshop*, JPL Publ. 90-54, Jet Propulsion Laboratory, Pasadena, CA, pp. 243–270.

Golub, G. H., and Van Loan, C. F. (1989), *Matrix Computations*, Johns Hopkins University Press, Baltimore, MD.

Hall, F. G., Botkin, D. B., Strebel, D. E., Woods, K. D., and Goetz, S. J. (1991), Large-scale patterns of forest succession as determined by remote sensing, *Ecology* 72:628–640.

Horowitz, H. M., Nalepka, R. F., Hyde, P. D., and Morganstern, J. P. (1971), Estimating the proportions of objects within a single resolution element of a Multispectral Scanner, University of Michigan, Ann Arbor, NASA Contract NAS-9-9784.

INPE (Instituto Nacional de Pesquisas Espaciais) (1992), *Deforestation in Brazilian Amazonia*, INPE, Sao Jose dos Campos, Brazil.

Lawler, M., and Adams, J. B. (1994). Characterizing image errors using the spectral mixture framework, *Lunar Planet. Sci.* XXV:779–780.

Lovejoy, T. E., and Bierregaard, R. O., Jr. (1990). Central Amazonian forests and the Minimum Critical Size of Ecosystems Project, in *Four Neotropical Rain Forests* (A. Gentry, Ed.), Yale University Press, New Haven, CT, pp. 60–74.

Lucas, R. M., Honzak, M., Foody, G. M., Curran, P. J., and Corves, C. (1993), Characterizing tropical secondary forests using multi-temporal Landsat sensor imagery, *Int. J. Remote Sens.* 14:3016–3067.

Nelson, B. W. (1994) Natural forest disturbance and change in the Brazilian Amazon, *Remote Sens. Rev.* 10:105–125.

Nelson, B. W., Kapos, V., Adams, J. B., Oliveira, W. J., Braun, O. P. G., and do Amaral, I. L. (1994), Forest disturbance by large blowdowns in the Brazilian Amazon, *Ecology* 75: 853–858.

Roberts, D. A., Adams, J. B., and Smith, M. O. (1990), Predicted distribution of visible and near-infrared radiant flux above and below a transmittant leaf, *Remote Sens. Environ.* 34:1–17.

Roberts, D. A., Smith M. O., Sabol, D. E., Adams, J. B., and Ustin, S. L. (1992), Mapping the spectral variability in photosynthetic and non-photosynthetic vegetation, soils, and shade using AVIRIS, in *Proc. Third Annual Airborne Geosci. (AVIRIS) Workshop*, JPL Publ. 92-14, Jet Propulsion Laboratory, Pasadena, CA, Vol. 1, pp. 38–40.

Roberts, D. A., Smith M. O., and Adams, J. B. (1993), Green vegetation, nonphotosynthetic vegetation and soils in AVIRIS data, *Remote Sens. Environ.* 44:255–269.

Sabol, D. E., Adams, J. B., and Smith, M. O. (1992a), Quantitative sub-pixel spectral detection of targets in multispectral images, *J. Geophys. Res.* 97:2659–2672.

Sabol, D. E., Roberts, D. A., Smith, M. O., and Adams, J. B. (1992b), Temporal variation in spectral detection thresholds of substrate and vegetation in AVIRIS images, in *Proc. Third Annual Airborne Geosci. (AVIRIS) Workshop*, JPL Publ. 92-14, Jet Propulsion Laboratory, Pasadena, CA, Vol. 1, pp. 132–134.

Shimabukuro, Y. E., Holben, B. N., and Tucker, C. J. (1994), Fraction images derived from NOAA AVHRR data for studying the deforestation in the Brazilian Amazon, *Int. J. Remote Sens.* 15:517–520.

Skole, D., and Tucker, C. (1993), Tropical deforestation and habitat fragmentation in the Amazon: satellite data from 1978 to 1988, *Science* 260:1905–1910.

Smith, M. O., Ustin, S. L., Adams, J. B., and Gillespie, A. R. (1990a), Vegetation in deserts: I. A regional measure of abundance from multispectral images, *Remote Sens. Environ.* 31:1–26.

Smith, M. O., Ustin, S. L., Adams, J. R., and Gillespie, A. R. (1990b), Vegetation in deserts: II. Environmental influences on regional abundance, *Remote Sens. Environ.* 31:27–52.

Smith, M. O., Adams, J. B., and Sabol, D. E. (1994a), Spectral mixture analysis: New strategies for the analysis of multispectral data, in *Imaging Spectrometry—A Tool for Environmental Observations* (J. Hill and J. Megier, Eds.), Euro Courses, Remote Sensing, Vol. 4, Kluwer Academic Publishers, pp. 125–143.

Smith M. O., Roberts, D., Hill, J., et al. (1994b), A new approach to determining spectral abundances of mixtures in multispectral images, in *Proc. IGARSS 1994*, Pasadena, CA.